Rapid Estimation of Rate Constants of Batch Processes Using On-Line SW-NIR

Sabina Bijlsma, D. J. Louwerse, and Age K. Smilde
Process Analysis and Chemometrics, Dept. of Chemical Engineering, University of Amsterdam, NL-1018 WV Amsterdam, The Netherlands

A method is presented for estimating reaction rate constants very rapidly from on-line short-wavelength near-infrared measurements. It can deal with a strong spectral overlap between the individual spectra of the species in the reacting system. For this an iterative curve-resolution method is combined with a nonlinear fitting procedure. This procedure also makes it possible to assess the quality of the estimated reaction rate constants. Simulations show that the method can be applied in cases with extreme spectral overlap of the individual spectra of the species. The procedure is applied in practice to an example with a strong spectral overlap. Reaction rate constants of the two-step epoxidation of 2,5-di-tert-butyl-1,4-benzoquinone were estimated. This method can lead to the application to on-line monitoring reaction rate constants.

Introduction

Short-wavelength near-infrared (SW-NIR) spectroscopy is a useful tool for monitoring on-line continuous and batch processes. SW-NIR encompasses the wavelength range 700–1,100 nm. The absorbances in this region are mainly caused by third overtone and combinations of IR bands originating from –CH, –NH, and –OH stretches.

There are some advantages and disadvantages in using SW-NIR for on-line monitoring. The extinction coefficients of the bands are very weak and the peaks are very broad, so SW-NIR is not a fingerprint area. Unknown and known interferences can also make the spectra more complicated. However, the use of long pathlengths can compensate for the weak extinction coefficients. Multivariate calibration techniques can overcome the problem of interferences if the spectra of the species are dissimilar enough. The book by Martens and Naes (1989) describes multivariate calibration techniques very well. Many aspects of (SW)-NIR have been extensively described by Workman (1996).

A major advantage of SW-NIR over NIR and IR is the potential use of fiber optics, which makes it possible to measure on-line while the instrument is located in another safe place, a good distance from the process. Using long pathlengths in SW-NIR ensures that the spectrum is more representative of the bulk, and that the spectrum is not disturbed by absorption of thin layers on the wall of the cell.

Several publications have included applications of SW-NIR spectroscopy for monitoring processes. Cavinato et al. (1990) used SW-NIR to find ethanol during the course of the fermentation process. The measurements were performed noninvasively. Aldridge et al. (1993a,b) used SW-NIR to monitor the free radical polymerization of methyl-methacrylate. The conversion was obtained by plotting one specific wavelength representing the monomer of the recorded spectra vs. reaction time. The kinetic parameters involved were not estimated in either article.

Deady et al. (1993) estimated the kinetic parameters for styrene polymerization. They used the pulsed laser photolysis (PLP) technique and the molecular weight distribution (MWD) to find the propagation rate constants and the chain length of the formed polymer. The results were verified using numerical kinetic simulations. Olaj and Schnöll-Bitai (1988, 1989) used PLP in different modifications, and gel permeation chromatography (GPC) to determine the kinetic parameters for polymerization reactions. They reported that spectroscopic techniques cannot be used to obtain conversions because of the low concentration of radicals produced by PLP and the overlapping bands. As will be shown in this article,

Correspondence concerning this article should be addressed to A. K. Smilde.

however, multivariate techniques can solve the problem of overlapping bands, and the low concentration problem can be solved by using cells with longer path lengths.

Kaufman et al. (1982) and Chrastil (1988, 1993) used their own concentration data on species of a reacting system in order to estimate the reaction rate constants by applying traditional curve fitting of the kinetic expressions to the concentration vs. time data. This traditional approach to estimating reaction rate constants has some disadvantages. Samples of the reacting system have to be taken during the reaction, and it is always necessary to measure the concentrations of these samples by using nuclear magnetic resonance (NMR), for example, which is time-consuming.

Kinetic parameters can also be obtained using SW-NIR. If spectra have been obtained during a certain time interval of a process and equations of the chemical kinetics of the process are available, curve resolution (Lawton and Sylvestre, 1971) can be used to find the spectral features using kinetic information. Curve resolution is a set of techniques based on the determination of qualitative information and the recovery of response profiles, for example, time profiles. Nowadays, new modifications of curve-resolution techniques and applications have been published (Tauler et al., 1993, 1994, 1995; Casassas et al., 1995; Lacorte et al., 1995). Reaction rate constants can be incorporated as unknown parameters in the curve-resolution method. An iterative least-square optimization procedure is necessary for estimating the values of these unknown parameters. If the stoichiometry of the reaction is known, iterative curve resolution can be used as a powerful chemometric tool for estimating reaction rate constants very rapidly. For processes with unknown stoichiometry, curve resolution can be combined with target factor analysis (Bonvin and Rippin, 1990; Harmon et al., 1995).

Sylvestre et al. (1974) contains the basic idea of estimating an unknown reaction rate constant using recorded spectra from an unimolecular irreversible reaction for a certain length of time and iterative curve resolution. Mayes et al. (1992) determined the reaction rate constants of the pseudo-first-order two-step epoxidation of 2,5-di-*tert*-butyl-1,4-benzoquinone using iterative curve resolution without quality assessment; they compared their results with those from Hairfield et al. (1985), who used NMR to obtain the corresponding reaction rate constants and the concentrations of the species involved in the reacting system. Shrager and Hendler (1982) and Frans and Harris (1984, 1985) determined several unknown parameters using different modifications of iterative curve resolution. A summary of the developments of incorporating unknown parameters into iterative curve-resolution methods between 1965 and 1986 can be found in Shrager (1986).

A new approach for estimating the concentration profile of a species was reported by Bjørsvik (1996). Spectra were recorded during the course of a reaction. Principal-component analysis was used to decompose the spectral data. From the scores and the reaction time, a reaction profile was obtained. However, this method can only be used if one species absorbs in the wavelength range being considered. Hence, this approach is very limited, as many processes are based on complicated reaction schemes. So far, articles on the applications of iterative curve-resolution methods have not paid much attention to the experimental errors and instrumental noise that contribute to the estimation of the unknown parameters.

In this article, a method is presented for very rapidly estimating reaction rate constants from on-line SW-NIR measurements using two different algorithms. This method has a few advantages over the traditional curve fitting of kinetic expressions to concentration vs. time data mentioned earlier. Using the proposed method, it is not necessary to take samples of the reacting system during the batch process run. Hence, it is not necessary to obtain concentration vs. time data. Therefore, a lot of time and the costs of sophisticated instruments and operators are saved. Moreover, the proposed method can be applied noninvasively. Also quality assessment of the estimated reaction rate constants can be investigated. Besides which, since the method only takes a few seconds, it can be used on-line in real time.

The background of the algorithms will be explained in detail. Some simulations with synthetic spectra from a simple two-step process are used to show that the method can be used to estimate unknown reaction rate constants in cases where the individual spectra of the species involved are extremely overlapped. Next, the procedure described is applied to a real example. The same batch process as described by Mayes et al. (1992)—the pseudo-first-order two-step epoxidation of 2,5-di-*tert*-butyl-1,4-benzoquinone—is monitored using SW-NIR. Mayes et al. (1992) did not estimate the quality of the estimated reaction rate constants.

The procedure for rapid estimation of reaction rate constants is applied to the recorded spectra analogous to Mayes et al. (1992) using two algorithms, a standard algorithm and an improved one. In order to perform quality assessment, upper and lower error bounds are estimated for the estimated reaction rate constants. The performance of the two different iterative curve-resolution algorithms will be compared for both the simulations and the real example.

Theory

In this section, two different iterative curve-resolution algorithms, combined with a nonlinear fitting procedure, are described. Validation of the estimated reaction rate constants and the jackknife method are also discussed.

Notation

Boldface capital characters denote matrices, boldface lower-case characters denote vectors, the superscript "T" denotes a transpose, a hat matrix represents an estimation of that matrix, a bar matrix represents a truncated matrix, and $\| X \|$ indicates the Frobenius or Euclidian norm of matrix X $(M * N)$ defined by Eq. 1, with $m = 1, 2, \ldots, M$ and $n = 1, 2, \ldots, N$:

$$\| X \| = \sqrt{\sum_{m=1}^{M} \sum_{n=1}^{N} |x_{mn}|^2} . \tag{1}$$

Curve resolution

Let the matrix A $(M * N)$ be a collection of spectra with M wavelengths during a certain time period N of a reacting

system; hence, every column in A denotes the spectrum recorded at a certain time. F $(N * C)$ is the matrix containing concentration time profiles of C species in the reacting system; hence, every column in F denotes the concentration time profile of a species. D $(M * C)$ is the matrix containing the pure spectra of the different species; hence, every column in D denotes the pure spectrum of a species. E $(M * N)$ is a matrix of errors. These errors can be divided into model errors, experimental errors, and instrumental noise. The following model can be built assuming Lambert-Beer's law (Burns and Ciurczak, 1992):

$$A = DF^T + E. \tag{2}$$

The dimensions of the matrices in Eq. 2 are shown in Figure 1.

Suppose that the following first-order consecutive reaction is considered to be the reaction model.

Step 1: $A \rightarrow B$, with reaction rate constant k_1.

Step 2: $B \rightarrow C$, with reaction rate constant k_2.

Equations 3, 4, and 5 are the kinetic rate equations describing the concentration profiles of species A, B, and C, respectively, initially with only A present:

$$C_{A,i} = C_{A,0} e^{-k_1 t_i} \tag{3}$$

$$C_{B,i} = \frac{k_1 C_{A,0}}{(k_2 - k_1)} \left(e^{-k_1 t_i} - e^{-k_2 t_i}\right) \tag{4}$$

$$C_{C,i} = C_{A,0} - C_{A,i} - C_{B,i}, \tag{5}$$

where $C_{A,i}$ is the concentration of species A at time i, and $C_{B,i}$ and $C_{C,i}$ are the concentrations for B and C, respectively; $C_{A,0}$ is the initial concentration of species A at time 0. The concentration profiles of A, B, and C are shown in Figure 2 for a simulated case, where $C_{A,0}$, k_1, and k_2 are equal to $0.39 \cdot 10^{-1}\text{mol}^{-1}$, 0.26 min^{-1}, and 0.07 min^{-1}, respectively.

If F is *known*, the corresponding reaction rate constants can be estimated by fitting the kinetic rate equations (Eqs. 3–5) to the time vs. concentration data. Suppose A is measured from a reacting system and F is *unknown* because there are no concentration data available. F can be constructed with the unknown reaction rate constants if a model for the kinetic rate equations and the initial concentrations of the species are available. Every column in F represents the reaction rate equation of a species with unknown reaction rate

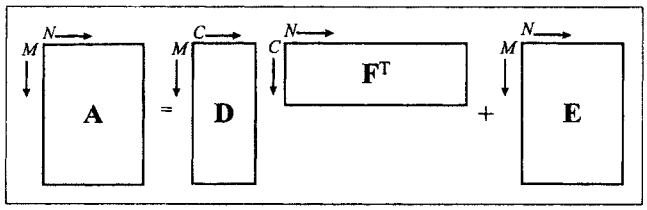

Figure 1. Visualization of the matrices and their dimensions involved in the applied iterative curve resolution procedure.

M = wavelengths; N = time points; C = species.

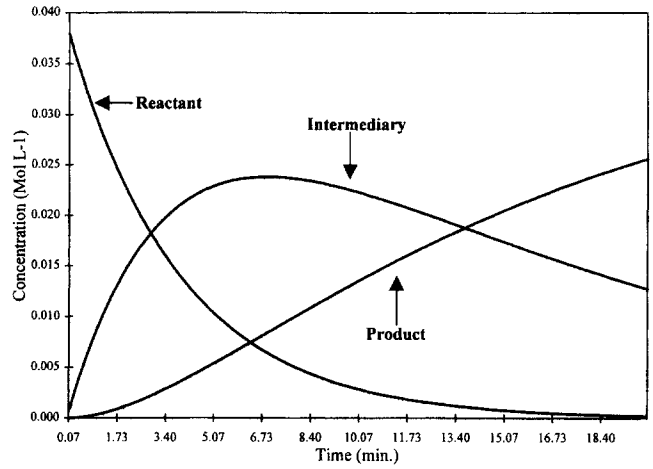

Figure 2. F matrix.

Concentration profiles of three species (reactant, intermediary, and product).

constant(s). If the unknown reaction rate constants are estimated, the concentration profiles can be reconstructed.

The matrix A can be described as the product of three matrices, called the singular-value decomposition (SVD) of A. Assuming $N \leq M$:

$$A = USV^T. \tag{6}$$

$U^TU = I$, $V^TV = VV^T = I$, U $(M * N)$, V $(N * N)$, and S is a $(N * N)$ diagonal matrix, with the singular values on the diagonal, arranged in decreasing order. For cases of $M < N$, the transpose A^T of A can be used.

Equation 6 can be truncated to the first C significant singular values. The truncated form of Eq. 6 is shown in Eq. 7:

$$\bar{A} = \bar{U}_C \bar{S}_C \bar{V}_C^T. \tag{7}$$

The dimensions of $\bar{A}$ in Eq. 7 are still $(M * N)$. The dimensions of the other matrices are $\bar{U}_C$ $(M * C)$ containing the first C columns of $\bar{U}$; $\bar{S}_C$ $(C * C)$ is the upper left part of $\bar{S}$; and $\bar{V}_C$ $(N * C)$ contains the first C columns of $\bar{V}$. Assuming Lambert-Beer's law, there are no model errors. Using Eq. 2, it is assumed that by using Eq. 7, E is greatly reduced. Hence, Eq. 8 follows:

$$\bar{A} = \hat{D}\hat{F}^T = \bar{U}_C \bar{S}_C \bar{V}_C^T. \tag{8}$$

Transposing Eq. 8:

$$\hat{F}\hat{D}^T = \bar{V}_C \bar{S}_C \bar{U}_C^T. \tag{9}$$

Since $\hat{F}$, $\bar{V}_C$, $\hat{D}^T$, and $\bar{S}_C\bar{U}_C^T$ are of full rank, Eq. 9 shows that the range of $\hat{F}$, $R(\hat{F})$ is equal to the range of $\bar{V}_C$, $R(\bar{V}_C)$. $R(\hat{F})$ represents the space spanned by the concentration profiles, and $R(\bar{V}_C)$ represents the abstract space spanning the concentration profiles. Hence, Eq. 9 can be rewritten as Eq.

10, where the superscript "+" indicates the Moore-Penrose inverse:

$$\hat{F}(\hat{D}^T)\left(\bar{S}_C\bar{U}_C^T\right)^+ = \bar{V}_C, \tag{10}$$

or

$$\hat{F}\hat{H} = \bar{V}_C, \tag{11}$$

where $\hat{F}\hat{H}$ spans the same space as $\bar{V}_C$.

If $\bar{V}_C$ is known from the SVD of matrix A and a model for $\hat{F}$ is known, $\hat{H}$ can be estimated according to Eq. 12. It is important to stress here that $\hat{F}$ itself is not known because there are no concentration data for the species available. A model for $\hat{F}$ is known because the kinetic expressions describing the concentration profiles of the species are known:

$$\hat{H} = (\hat{F}^T\hat{F})^{-1}\hat{F}^T\bar{V}_C, \tag{12}$$

where the superscript "-1" indicates the inverse.

$\hat{F}$ is fixed by reaction rate constants k_1 and k_2. Hence, if these constants are correct, Eq. 11 should hold exactly with the corresponding $\hat{H}$ from Eq. 12. Therefore, it is reasonable to minimize Eq. 13 over k_1 and k_2, ensuring that for the proper k_1 and k_2 this minimum of zero will be attained:

$$\min_{\hat{F}} \| \bar{V}_C - \hat{F}\hat{H} \|^2 = \min_{\hat{F}} \| \left[I - \hat{F}(\hat{F}^T\hat{F})^{-1}\hat{F}^T \right] \bar{V}_C \|^2$$

$$= \min_{k_1,k_2} \| \left[I - \hat{F}(\hat{F}^T\hat{F})^{-1}\hat{F}^T \right] \bar{V}_C \|^2, \tag{13}$$

where $\bar{V}_C$ is fixed; I is the identity; and $\hat{F}$ depends on k_1 and k_2. Equation 14 represents a more sophisticated version of Eq. 13 by weighting the columns of $\hat{V}_C$ to account for the differences in error in the columns of $\bar{V}_C$ (Shrager, 1986). Equation 14 can be valuable if data are very noisy:

$$\min_{\hat{F}} \| \bar{V}_C\bar{S}_C - \hat{F}\hat{H}\bar{S}_C \|^2 = \min_{\hat{F}} \| \left[I - \hat{F}(\hat{F}^T\hat{F})^{-1}\hat{F}^T \right] \bar{V}_C\bar{S}_C \|^2$$

$$= \min_{k_1,k_2} \| \left[I - \hat{F}(\hat{F}^T\hat{F})^{-1}\hat{F}^T \right] \bar{V}_C\bar{S}_C \|^2. \tag{14}$$

Equations 13 and 14 are both nonlinear in k_1 and k_2, and therefore they should be minimized using iterative nonlinear least squares. In this article the Levenberg-Marquardt algorithm was used (Seber and Wild, 1989; Press et al., 1992). The minimalization procedure in Eqs. 13 and 14 is done according to the following scheme.

Initializing

1) Use a starting value for both k_1 and k_2.

2) Reconstruct the concentration profile of the different species using the starting values from step 1. Hence, construct $\hat{F}$.

3) Calculate $\| [I - \hat{F}(\hat{F}^T\hat{F})^{-1}\hat{F}^T]\bar{V}_C\bar{S}_C \|^2$.

Minimalization loop

4) Modify the reaction rate constants according to the Levenberg-Marquardt method.

5) Reconstruct the concentration profile of the different species using the modified values of the reaction rate constants from step 4.

6) Calculate $\| [I - \hat{F}(\hat{F}^T\hat{F})^{-1}\hat{F}^T]\bar{V}_C\bar{S}_C \|^2$.

7) Compare the value obtained from step 3 with the value of step 6.

8) Repeat the minimalization loop until the convergence criterion is reached.

Equations 13 and 14 have been used in this article to estimate the reaction rate constants. For convenience, Eqs. 13 and 14 will be labeled "the standard algorithm" and "the weighted algorithm," respectively. If iterative techniques are used, the order of magnitude of the reaction rate constants has to be known in advance, because of the starting values for the reaction rate constants in the algorithm. The Levenberg-Marquardt algorithm can stop in a local minimum if bad starting values are used. If different sets of starting values are used, this can be checked. However, if the order of magnitude of the reaction rate constants is not known in advance, there are several algorithms available to generate acceptable starting values (Seber and Wild, 1989). In this article we chose values close to the estimations for the reaction rate constants from Mayes et al. (1992).

If the reaction rate constants are estimated, the fit error can be calculated according to Eq. 15 for the standard algorithm and Eq. 16 for the weighted algorithm.

Standard algorithm:

$$\text{Fit error} = \frac{\| \bar{V}_C - \hat{F}\hat{H} \|}{\| \bar{V}_C \|} \times 100\%. \tag{15}$$

Weighted algorithm:

$$\text{Fit error} = \frac{\| \bar{V}_C\bar{S}_C - \hat{F}\hat{H}\bar{S}_C \|}{\| \bar{V}_C\bar{S}_C \|} \times 100\%. \tag{16}$$

A value of 0% for both equations indicates that there are no residuals.

Both of the algorithms described here are very fast. The whole procedure only takes a few seconds. Because the algorithms are iterative, the exact speed is not known in advance, so the choice of the starting values plays a crucial role.

Quality assessment of the estimated reaction rate constants

Assume that n repeated individual batch process runs are performed under identical conditions. Normally, the reaction rate constants are estimated from the mean batch process runs obtained by averaging all the repeated individual batch process runs. The error of the estimates is unknown in this case. If reaction rate constants are estimated for several repeated individual batch process runs, however, there will be some fluctuations between these estimations. This can be caused by model errors, experimental errors, and instrumental noise.

The model errors can be kept to a minimum if the correct kinetic model is used and the law of Lambert-Beer is valid. Experimental errors and instrument noise are always present.

For example, experimental errors are caused by concentration errors and errors due to the starting point of the reaction, while instrumental noise is caused by variations in the instrument. It is possible to reduce experimental errors, but instrumental noise is inevitable. An upper level of the individual standard deviation of the estimated reaction rate constants due to experimental errors and instrument noise, the upper error bound, can be estimated by following the following procedure.

Assume a batch process with one reaction step and reaction rate constant k_1. For each individual batch process run, the reaction rate constant k_1 can be estimated. A mean and individual standard deviation can be obtained from the k_1 estimations of the n repeated individual batch process runs. The individual standard deviation obtained represents the upper error bound, which is the worst case, because both experimental errors and instrumental noise are involved.

A lower level of the individual standard deviation, the lower error bound, represents the influence of the instrument noise on the k_1 estimates. It can be estimated using the jackknife method (Shao and Tu, 1995). The theory of the jackknife method is briefly explained in the next section.

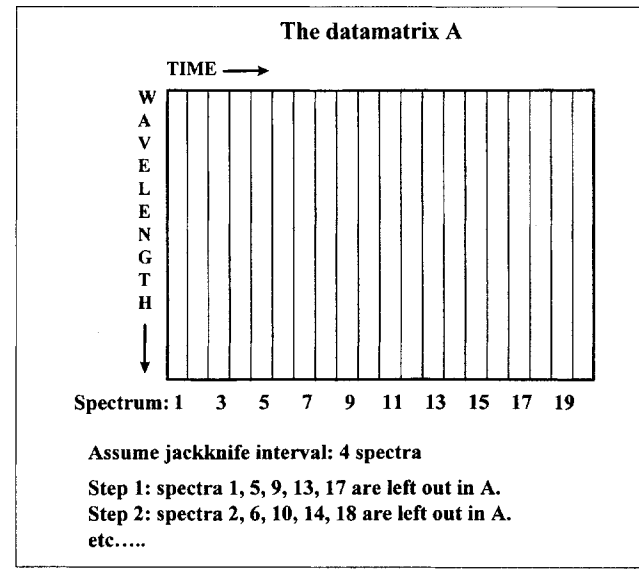

Figure 3. Visualization of the jackknife method.

Jackknife

Again assume a batch process with one reaction step and reaction rate constant k_1. Suppose every individual batch process run consists of recording 20 spectra during a certain time period. The mean batch process run (datamatrix A) can be obtained by averaging all the repeated individual batch process runs. Experimental errors and some instrumental noise are averaged. Hence, mainly instrumental noise is left. In the jackknife procedure, a fixed number of spectra from the mean batch process run are removed according to a fixed interval and k_1 is estimated using the remaining spectra. Next, another set of spectra is removed from the mean batch process run and k_1 is estimated again on the basis of the remaining spectra, and so on. Finally, a number of estimations for k_1 are obtained for the mean batch process run. Both a mean and individual standard deviation can be obtained from the jackknife estimations. The individual standard deviation of the estimated k_1 represents the influence of the instrumental noise (lower error bound) to the k_1 estimates. The jackknife procedure is shown in Figure 3.

Simulations

The first-order two-step reaction described in the Theory section was used for the simulations. Concentration profiles were simulated for 21 time points for the species A, B, and C, corresponding to a k_1 value of 0.30 min^{-1}, a k_2 value of 0.05 min^{-1}, and an initial concentration of A of 1 mol l^{-1}. The time period chosen was from 0 min to 20 min with increments of 1 min. Pure SW-NIR spectra were simulated for the three individual species for the wavelength range 850–1,050 nm with increments of 1 nm using Gaussian peaks with a peak sigma of 15 nm. To control the amount of spectral overlap of the three peaks, the peak maximum of the A, B, and C species corresponded to different wavelengths. The simulated spectra for the data matrix A were calculated using Eq. 2. Normally distributed white noise was added to the data matrix A. The sigma of the white noise was defined as a percentage of the maximum absorbance of the simulated SW-NIR spectrum at time 0.

Some simulations were performed with the standard and weighted algorithm to show the performance of the iterative curve resolution combined with a nonlinear fitting procedure. The amount of overlap in the individual SW-NIR spectra of the different species involved was varied by moving the individual spectra of species A and C along the wavelength axis. The pure spectra of the individual species with a small and a strong overlap are shown in Figure 4. A small overlap corresponded to a peak maximum of 900 nm, 950 nm, and 1,000 nm for the species A, B, and C, respectively, while a strong overlap corresponded to a peak maximum of 930 nm, 950 nm, and 970 nm for the same species, respectively. Two different noise levels (1% and 4%) were used to simulate 100 sets of SW-NIR spectra. For data reduction with the SVD, three singular values were chosen, because three species are involved in the simulated SW-NIR spectra. For every noise level, 100 k_1 and k_2 values were estimated. The starting values for k_1 and k_2 were always 0.20 min^{-1} and 0.04 min^{-1}, respectively.

Experimental Studies

Reaction

The following two-step epoxidation of 2,5-di-*tert*-butyl-1,4-benzoquinone using *tert*-butyl hydroperoxide and benzyltrimethylammonium hydroxide (Triton B) catalyst was used as an example process for experiments (Hairfield et al., 1985; Mayes et al., 1992):

Step 1: $A + B \rightarrow C + D$, with reaction rate constant k_1.

Step 2: $C + B \rightarrow D + E$, with reaction rate constant k_2.

The species A, B, C, D, and E are specified in Table 1.

Because the spectral differences between the *cis* and *trans* product are negligible in SW-NIR, no distinction was made between these two species. If the *tert*-butyl hydroperoxide is present in large amounts, pseudo-first-order kinetics can be assumed. Hence, the kinetic equations (Eqs. 3, 4, 5) can be

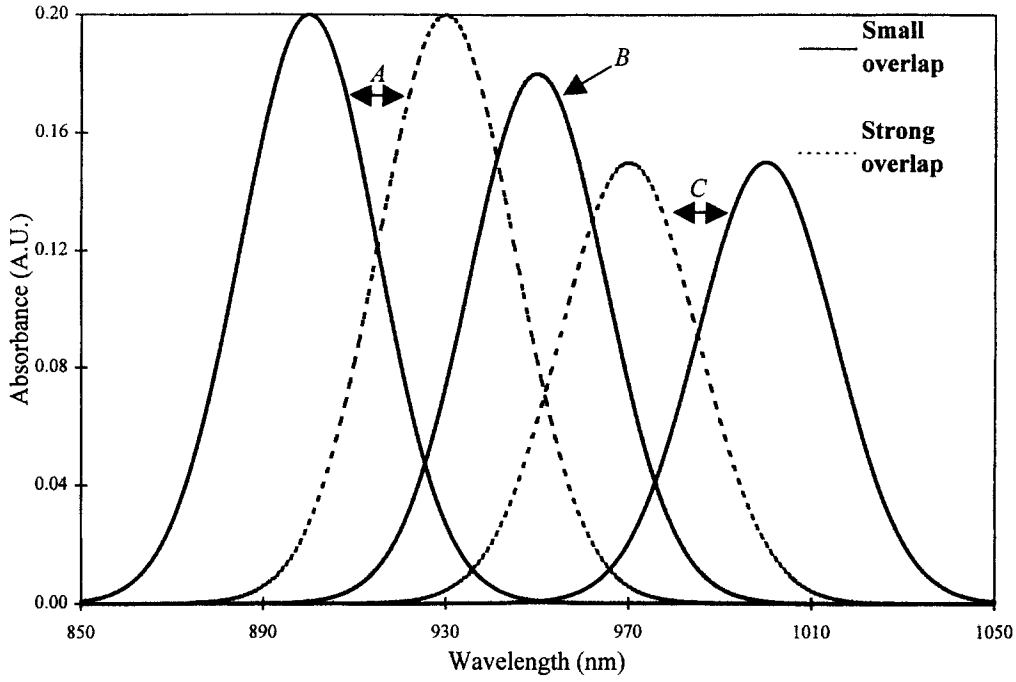

Figure 4. Pure spectra of the individual species *A*, *B*, and *C* for the SW-NIR simulations.

The peak of species *B* is the same for the small and strong overlap.

used to describe the concentration profiles of the spectroscopic active species *A*, *C*, and *E*, respectively. In this article, *A*, *C*, and *E* are monitored; they represent the reactant, intermediary, and main product of the reaction being considered.

Reagents

The 2,5-di-*tert*-butyl-1,4-benzoquinone was synthesized from the procedure described by Hairfield et al. (1985) with no further purification, and a melting point for it of 152–153°C was obtained. The reported melting point is 152.5°C (Weast, 1988).

Sample preparation

First, 0.264 g (1.2 mmol) of 2,5-di-*tert*-butyl-1,4-benzoquinone was dissolved in 15-mL dioxane (Acros Chimica, 99$^+$%). When solution was complete, 1.55 mL of the *tert*-butylhydroperoxide 70% (Acros Chimica) solution in water (12 mmol) and 13.21 mL ethanol (BDH Laboratory Supplies, pro analysis) were added. The curvette was filled with the reaction mixture. When the temperature in the cuvette had reached the target temperature, data collection was started upon addition of 0.24 mL of the ice-cold catalyst Triton B (Acros Chimica, 40 wt. % in methanol) in 0.50-mL ethanol and 0.60-mL dioxane. The Triton-B was mixed with dioxane and ethanol so that the whole reaction mixture would mix rapidly. Ice-cold Triton-B was used to stabilize the temperature in the cuvette.

Table 1. Species Involved in the Two-Step Epoxidation of 2,5-di-*tert*-Butyl-1,4-Benzoquinone

A	2,5-di-*tert*-butyl-1,4-benzoquinone
B	*tert*-butyl hydroperoxide
C	2,5-di-*tert*-butyl mono-epoxide-1,4-benzoquinone
D	*tert*-butyl alcohol
E	*cis* and *trans* 2,5-di-*tert*-butyl di-epoxide-1,4-benzoquinone

Experimental setup

The experimental setup is shown in Figure 5. A Hewlett-Packard 8453 UV-VIS spectrophotometer with diode array

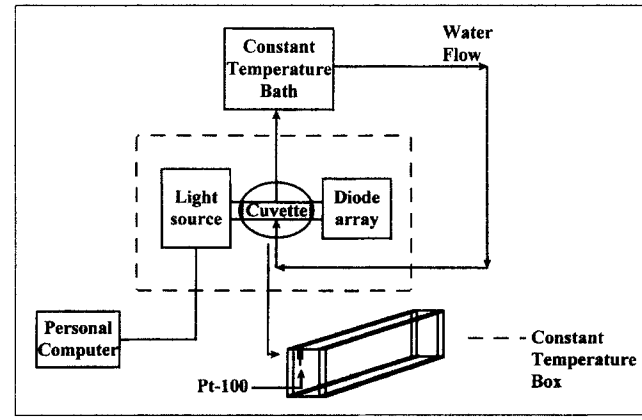

Figure 5. Experimental setup.

The light source, cuvette, and diode array are inside the constant-temperature box.

detection was used to measure the SW-NIR spectra. A quartz cuvette with a 10.00-cm pathlength (Hellma Benelux) was used to obtain the spectra of the reaction mixture. A small unit of glass was glued to each side of the cuvette to regulate the temperature in the cuvette. The cuvette contained two stirring modules. Water was pumped from a constant-temperature bath (Neslab) through the cooling units of the cuvette. A Pt-100, which is a thermocouple, connected to the constant-temperature bath was used inside the cuvette to control the temperature. To obtain a temperature below room temperature, an immersion cooler (Haake) was used to cool the water of the constant-temperature bath.

The cuvette was placed in a specially constructed cell holder. The spectrophotometer and the cuvette were then placed in a homemade air thermostated box, to avoid the influence of the temperature fluctuations in its outside surroundings. The box temperature was controlled by a constant-temperature bath (Haake). A Hewlett-Packard Vectra XM2 Chemstation (IntelDX4—100 MHz with 16 MB RAM and an 800 MB hard disk), using Hewlett-Packard software, collected and stored the data. The experimental conditions are listed in Table 2. Eight individual batch process runs were performed.

Reproducibility

There reproducibility, R_{batch}, of the eight individual batch process runs was obtained using the following expression (Smilde et al., 1994):

$$R_{\text{batch}} = \frac{\sqrt{\frac{1}{n}\sum_{i=1}^{n} \| \boldsymbol{A}_i - \boldsymbol{A}_m \|^2}}{\| \boldsymbol{A}_m \|} \times 100\%, \qquad (17)$$

where $\boldsymbol{A}_i$ is the data matrix for process run i and $\boldsymbol{A}_m$ is the averaged raw data matrix estimated for n individual batch process runs according to Eq. 18:

$$\boldsymbol{A}_m = \frac{1}{n}\sum_{i=1}^{n} \boldsymbol{A}_i. \qquad (18)$$

The reproducibility R_{time} for every recorded spectrum at time t was obtained according to the following expression:

$$R_{\text{time}(t)} = \frac{\sqrt{\frac{1}{n}\sum_{i=1}^{n} \| \boldsymbol{a}_{i,t} - \boldsymbol{a}_{m,t} \|^2}}{\| \boldsymbol{a}_{m,t} \|} \times 100\%, \qquad (19)$$

Table 2. Experimental Conditions

Reaction temperature	17°C
Integration time*	1 s
Sampling time	5 s
Total run time	1,200 s
Wavelength range	800–1,100 nm
Wavelength interval	1.0 nm
No. of recorded spectra	240

*It took 1 s to measure 10 spectra from 800 to 1,100 nm. These spectra were averaged.

where $\boldsymbol{a}_{i,t}$ is the raw spectrum for process run i at time t, and $\boldsymbol{a}_{m,t}$ is the averaged raw spectrum m at time t estimated for n individual batch process runs according to Eq. 20:

$$\boldsymbol{a}_{m,t} = \frac{1}{n}\sum_{i=1}^{n} \boldsymbol{a}_{i,t}. \qquad (20)$$

Data processing

In order to remove base line effects and drift, second-derivative spectra were estimated using a Savitzky-Golay filter (Savitzky and Golay, 1964), as the usual procedure for estimating a second derivative will result in noisy spectra. For the Savitzky-Golay filtering, a window of 15 data points was used. At this window size, the spectral characteristics are kept and the noise level is reduced. The main spectral features are caused by dioxane, ethanol, and the catalyst. To stress the spectral features of the appearing and disappearing species, second-derivative difference spectra were calculated after subtracting the fourth recorded spectrum, the blank, from all the other spectra. The reason for this is given in the Results and Discussion section.

The second-derivative difference spectra were used to apply the iterative curve-resolution algorithms combined with a nonlinear fitting procedure, as described in the Theoretical section. The entire wavelength range of the second-derivative difference spectra was not used for data processing because of the increasing absorbance of the byproduct *tert*-butyl alcohol formed during the reaction and the decreasing absorbance of *tert*-butylhydroperoxide. The spectral features are caused by the three benzoquinone species if the 860–880-nm wavelength is considered (Mayes et al., 1992). For data reduction, obtained using a SVD, three singular values were used because three species are involved in the selected wavelength range and linearity and additivity is assumed. Because of imbedded error, it might be better to truncate to four singular values. Since the fourth singular value is quite small, however, it is reasonable to truncate to three singular values.

Data processing was performed in the Matlab environment (Version 4.2C, The Mathworks Inc.) on a Pentium 90-MHz personal computer with 32-MB RAM and a 800-MB hard disk.

Results and Discussion

Simulations

For the standard and weighted algorithms, 0.20 min^{-1} and 0.04 min^{-1} were used as starting value for k_1 and k_2, respectively. The mean values of the estimated parameters, k_i and $\hat{k}_2$, and the corresponding individual standard deviations are listed in Table 3 for both algorithms. From the values of both algorithms used, it is clear that a higher noise level will result in a larger individual standard deviation (high estimation error) for both reaction rate constants. If the noise level is constant and the spectral overlap is varied, the individual standard deviations of the reaction rate constants become larger. However, the iterative curve resolution can still be applied successfully if there is a large amount of overlap in the individual spectra of the different species.

If the values for the standard algorithm are compared to the values for the weighted algorithm, it is clear that there is

Table 3. Mean Estimated k_1 and k_2 Values with Individual Standard Deviations for 100 Simulated Sets of SW-NIR Spectra with Two Noise Levels and Four Spectral Overlaps*

$P_{max,A}$ (nm)	$P_{max,B}$ (nm)	$P_{max,C}$ (nm)	Noise Level (%)	Mean k_1 (min^{-1})	Mean k_2 (min^{-1})	STD k_1 (min^{-1})	STD k_2 (min^{-1})
900	950	1,000	1	0.2999 (0.3000)	0.0500 (0.0497)	0.0034 (0.0021)	0.0026 (0.0018)
			4	0.2993 (0.2998)	0.0510 (0.0504)	0.0123 (0.0073)	0.0085 (0.0075)
910	950	990	1	0.2997 (0.2997)	0.0500 (0.0502)	0.0035 (0.0023)	0.0027 (0.0019)
			4	0.2994 (0.3013)	0.0511 (0.0497)	0.0139 (0.0080)	0.0115 (0.0082)
920	950	980	1	0.2999 (0.3001)	0.0501 (0.0498)	0.0038 (0.0025)	0.0031 (0.0023)
			4	0.2997 (0.2981)	0.0506 (0.0516)	0.0157 (0.0091)	0.0127 (0.0089)
930	950	970	1	0.2994 (0.3000)	0.0501 (0.0498)	0.0059 (0.0032)	0.0043 (0.0028)
			4	0.2971 (0.3001)	0.0507 (0.0501)	0.0305 (0.0138)	0.0181 (0.0115)

*$P_{max,i}$ indicates the spectral position of the peak maximum of species i. The values are obtained with the standard algorithm. The values in parentheses are obtained with the weighted algorithm. If different sets of starting values were used, similar results were obtained. Here 0.20 min^{-1} and 0.04 min^{-1} were used as starting values for k_1 and k_2, respectively.

an improvement in the individual standard deviations for both k_1 and k_2 if the weighted algorithm is used. Hence, using the weighted algorithm is extremely valuable if data are very noisy.

Experiments

Reproducibility. The reproducibility of the raw spectra is 3.55% using Eq. 17. Figure 6 contains the raw spectra of one individual batch process run. From this figure, it is clear that a few spectra do not match with the other spectra. These spectra are the first spectra recorded just after the catalyst was added. It is assumed that the reaction mixture is not homogeneous, because it takes some time to mix very well. The calculated reproducibility vs. the spectrum number is shown in Figure 7. From Figure 7, it is clear that the first two or three spectra had to be deleted. In fact, three spectra were deleted, and the fourth spectrum was used as blank.

The Savitzky-Golay filtered second-derivative spectra of Figure 6 are shown in Figure 8, and the second-derivative difference spectra of Figure 8 are shown in Figure 9. There is a trend in the successive spectra. The reproducibility of the second-derivative difference spectra is 23.38%. This lower reproducibility is mainly a consequence of the small differences in absorbances of the species and the error propagation caused by taking the second derivative.

Reaction Rate Constants Estimations. The mean data matrix was obtained by averaging the data matrices of the eight repeated individual batch process runs. The k_1 and k_2 values were estimated with the standard and weighted algorithms using starting values of 0.30 min^{-1} and 0.05 min^{-1} for k_1

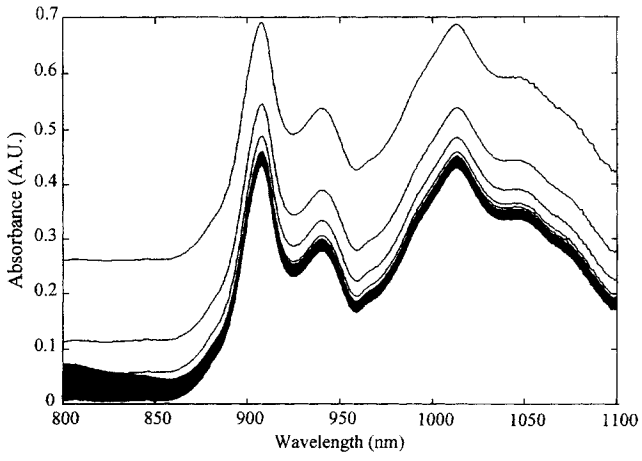

Figure 6. Raw spectra from one individual batch process run.

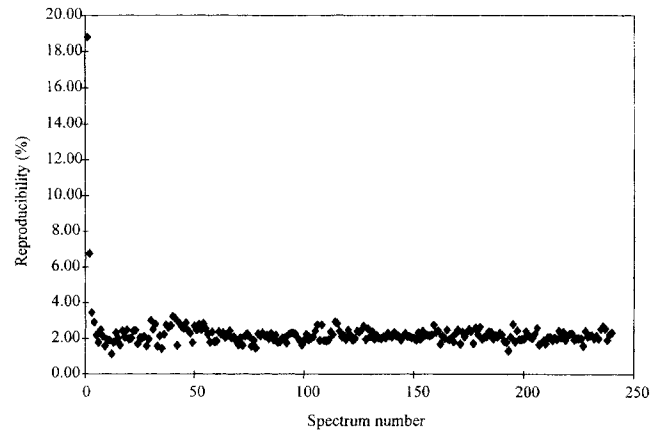

Figure 7. Reproducibility vs. spectrum number.

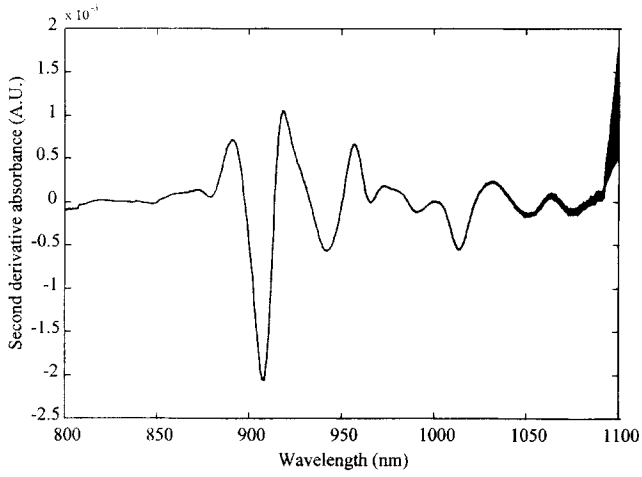

Figure 8. Second derivative spectra from Figure 6; the first three spectra are deleted.

and k_2, respectively. These values are the results from Mayes et al. (1992), based on only two repeated individual batch process runs using the standard algorithm. If other starting values were used, similar results were obtained. The fit errors were also estimated, and the results are listed in Table 4. The kinetic model is satisfactory, because the fit error is small.

Estimation of the Upper Error Bound. In order to obtain individual standard deviations of the estimated reaction rate constants, the procedure as explained in the Theory section was applied. One k_1 and one k_2 value were estimated for the eight repeated individual batch runs using a starting value of 0.30 min^{-1} and 0.05 min^{-1} for k_1 and k_2, respectively. If other starting values were used, similar results were obtained. The mean values obtained for both the standard and weighted algorithms with individual standard deviations are listed in the first part of Table 5. From Table 5, it is clear that the estimated reaction rate constants from Mayes et al.

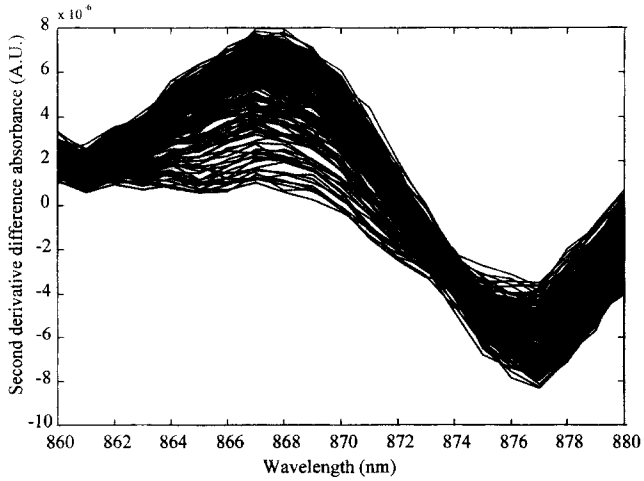

Figure 9. Second derivative difference spectra from Figure 8 for the wavelength range 860–880 nm.

Table 4. Estimated Reaction Rate Constants for the Mean Data Matrix Obtained Over Eight Averaged Individual Batch Process Runs*

Starting Value k_1 (min^{-1})	Starting Value k_2 (min^{-1})	Est. k_1 (min^{-1})	Est. k_2 (min^{-1})	Fit Error (%)
0.30	0.05	0.30 (0.26)	0.04 (0.07)	2.59 (2.63)

*The values are obtained with the standard algorithm. The values in parentheses are obtained with the weighted algorithm. If different sets of starting values were used, similar results were obtained.

(1992) are within the 95% confidence limits for the estimations obtained in this article. The individual standard deviations in the first part of Table 5 represent the upper error bound (worst case), because both experimental errors and instrumental noise are involved. Hence, there is no averaging effect. From Table 5, it is clear that the weighted algorithm performs better for k_1 than the standard algorithm. There is a factor of 3 improvement in individual standard deviation for the k_1 estimations, while for both algorithms the individual standard deviations are quite large for k_2. This is due to the dominance of k_1 and the high noise level present in the data.

In the preceding procedure, the correlation between the eight k_1 and the eight k_2 estimations for both algorithms was estimated. The correlation coefficient is -0.77 if the standard algorithm was used, and -0.61 if the weighted algorithm was used. Because of this moderate correlation between the estimated k_1 and k_2 values, the k_1 estimations tend to be too high when the k_2 estimations are too low, and vice versa. The reconstructed concentration profiles for the three benzoquinone species are shown in Figure 2 for when the estimations of the reaction rate constants obtained for the upper error bound with the weighted algorithm from Table 5 are used.

Estimation of the Lower Error Bound. The lower error bound was estimated using the jackknife procedure described in the Theory section. Spectra were left out of the mean batch run using an interval of 31. Finally, this resulted in ten jack-

Table 5. Mean Estimated k_1 and k_2 Values and Individual Standard Deviation According to the Upper and Lower Error Bound*

Type of Error Bound	Starting Value k_1 (min^{-1})	Starting Value k_2 (min^{-1})	Mean* k_1 (min^{-1})	Mean* k_2 (min^{-1})	STD k_1 (min^{-1})	STD k_2 (min^{-1})
Upper	0.30	0.05	0.31 (0.26)	0.05 (0.07)	0.09 (0.03)	0.03 (0.03)
Lower	0.30	0.05	0.30 (0.26)	0.04 (0.07)	6.80×10^{-3} (1.00×10^{-3})	3.10×10^{-3} (1.80×10^{-3})

*The values are obtained with the standard algorithm. The values in parentheses are obtained with the weighted algorithm. Mean over eight values. In case of jackknife results it is the mean over ten jackknife estimations. If different sets of starting values were used, similar results were obtained.

knife estimations for k_1 and k_2 for the averaged batch run. The jackknife procedure was applied to the standard and weighted algorithms using starting values of 0.30 min^{-1} and 0.05 min^{-1} for k_1 and k_2, respectively. If other starting values were used, similar results were obtained. The mean value obtained for the reaction rate constants and the corresponding individual standard deviation for the standard and weighted algorithms are listed in the last part of Table 5. The estimated individual standard deviation (lower error bound) represents the influence of the instrumental noise on the reaction rate constant estimates. There is an improvement in individual standard deviation for both k_1 and k_2 estimations (factors of 7 and 2, respectively) if the weighted algorithm is used.

Summary of Results. Using the weighted algorithm, the mean estimated k_1 value is 0.26 min^{-1}, with an error between $1.00 \cdot 10^{-3}$ min^{-1} (lower error bound) and 0.03 min^{-1} (upper error bound). With this algorithm, the mean estimated k_2 value is 0.07 min^{-1}, with an error between $1.80 \cdot 10^{-3}$ min^{-1} (lower error bound) and 0.03 min^{-1} (upper error bound). These values show that it is possible to estimate the reaction rate constants with good precision even in the case where there is high spectral overlap and a high noise level. For all k_1 and k_2 estimations, k_1 estimations that are too high tend to occur with k_2 estimations that are too low, and vice versa due to the moderate correlation (-0.61).

Conclusions

Reaction rate constants of batch processes can be estimated from on-line SW-NIR measurements. To estimate the reaction rate constants, an improved algorithm was used. The two-step epoxidation of 2,5-di-*tert*-butyl-1,4-benzoquinone was used as an example batch process to illustrate that the algorithm can be used if there is a strong spectral overlap of the individual spectra of the different species and a high noise level. Reaction rate constants were estimated using the recorded SW-NIR spectra from the reacting system. One big advantage the described procedure has is the rapid estimation of the reaction constants. Also the upper and lower error bounds of the reaction rate constants can be estimated, which is very important for quality assessment. Simulations showed that the presented algorithm can be applied successfully in the case where there is an extreme overlap of the spectra of the individual species involved.

Because of the rapid estimation of the reaction rate constants from on-line SW-NIR measurements, the procedure presented in this article can have many applications in the areas of obtaining information about batch processes and statistical control of batch processes. Expanding to more complicated processes, such as batch polymerization processes, is also possible. In the future, the procedure described in this article can be valuable for on-line monitoring of reaction rate constants.

Acknowledgment

The authors thank the people from the mechanical workshop and the glassworks for construction of the cell holder and the cooling units of the cuvette, respectively.

Literature Cited

Aldridge, P. K., D. H. Burns, J. J. Kelly, and J. B. Callis, "Monitoring of Methyl Methacrylate Polymerization Using Non-Invasive SW-NIR Spectroscopy," *Process Control Qual.*, **4**, 155 (1993a).

Aldridge, P. K., J. J. Kelly, D. H. Burns, and J. B. Callis, "Noninvasive Monitoring of Bulk Polymerization Using Short-Wavelength Near-Infrared Spectroscopy," *Anal. Chem.*, **65**, 3581 (1993b).

Bjørsvik, H.-R., "Reaction Monitoring in Explorative Organic Synthesis Using Fiber-Optical NIR Spectroscopy and Principal Component Analysis," *Appl. Spectrosc.*, **50**, 1541 (1996).

Bonvin, D., and D. W. T. Rippin, "Target Factor Analysis for the Identification of Stoichiometric Models," *Chem. Eng. Sci.*, **45**, 3417 (1990).

Burns, D. A., and E. W. Ciurczak, *Handbook of Near-Infrared Analysis*, Marcel Dekker, New York (1992).

Casassas, E., I. Marqués, and R. Tauler, "Study of Acid-Base Properties of Fulvic Acids Using Fluorescence Spectrometry and Multivariate Curve Resolution Methods," *Anal. Chim. Acta*, **310**, 473 (1995).

Cavinato, A. G., D. M. Mayes, Z. Ge, and J. B. Callis, "Noninvasive Method for Monitoring Ethanol in Fermentation Processes Using Fiber-Optic Near-Infrared Spectroscopy," *Anal. Chem.*, **62**, 1977 (1990).

Chrastil, J., "Determination of the First Order Consecutive Reaction Rate Constants from Final Product," *Comput. Chem.*, **12**, 289 (1988).

Chrastil, J., "Determination of the First Order Consecutive Reversible Reaction Kinetics," *Comput. Chem.*, **17**, 103 (1993).

Deady, M., A. W. H. Mau, G. Moad, and T. H. Spurling, "Evaluation of the Kinetic Parameters for Styrene Polymerization and Their Chain Length Dependence by Kinetic Simulation and Pulsed Laser Photolysis," *Makromol. Chem.*, **194**, 1691 (1993).

Frans, S. D., and J. M. Harris, "Reiterative Least-Squares Spectral Resolution of Organic Acid/Base Mixtures," *Anal. Chem.*, **56**, 466 (1984).

Frans, S. D., and J. M. Harris, "Least Squares Singular Value Decomposition for the Resolution of pK's and Spectra from Organic Acid/Base Mixtures," *Anal. Chem.*, **57**, 1718 (1985).

Hairfield, E. M., E. W. Moomaw, R. A. Tamburri, and R. A. Vigil, "The Epoxidation of 2,5-di-*tert*-butyl-1,4-benzoquinone," *J. Chem. Educ.*, **62**, 175 (1985).

Harmon, J. L., Ph. Duboc, and D. Bonvin, "Factor Analytical Modeling of Biochemical Data," *Comput. Chem. Eng.*, **19**, 1287 (1995).

Kaufman, D., C. Sterner, B. Masek, R. Svenningsen, and G. Samuelson, "An NMR Kinetics Experiment," *J. Chem. Educ.*, **59**, 885 (1982).

Lacorte, S., D. Barceló, and R. Tauler, "Determination of Traces of Herbicide Mixtures in Water by On-Line Solid-Phase Extraction Followed by Liquid Chromatography with Diode-Array Detection and Multivariate Self-Modelling Curve Resolution," *J. Chromatog. A*, **697**, 345 (1995).

Lawton, W. H., and E. A. Sylvestre, "Self Modeling Curve Resolution," *Technometrics*, **13**, 617 (1971).

Martens, H., and T. Naes, *Multivariate Calibration*, Wiley, Chichester (1989).

Mayes, D. M., J. J. Kelly, and J. B. Callis, "Non-Invasive Monitoring of a Two-Step Sequential Chemical Reaction with Shortwave Near-Infrared Spectroscopy," *Near Infra-Red Spectroscopy: Bridging the Gap between Data Analysis and NIR Applications*, K. I. Hildrum, T. Isaksson, T. Naes, and A. Tandberg, eds., Horwood, Chichester (1992).

Olaj, O. F., and I. Schnöll-Bitai, "The Laser-Flash-Initiated Polymerization as a Tool of Evaluating (Individual) Kinetic Constants of Free-Radical Polymerization, 4[a]: An Experimental Set-Up Capable of a Direct Determination of the Rate Constant of Termination k_t," *Makromol. Chem.*, **9**, 275 (1988).

Olaj, O. F., and I. Schnöll-Bitai, "Laser-Flash-Initiated Polymerization as a Tool for Evaluating (Individual) Kinetic Constants of Free-Radical Polymerization: 5. Complete Analysis by Means of a Single Experiment," *Eur. Polym. J.*, **25**, 635 (1989).

Press, W. H., S. A. Teukolsky, W. T. Vetterling, and B. P. Flannery, *Numerical Recipes*, Cambridge Univ. Press, New York (1992).

Savitzky, A., and M. J. E. Golay, "Smoothing and Differentiation of

Data by Simplified Least Squares Procedures," *Anal. Chem.*, **36**, 1627 (1964).
Seber, G. A. F., and C. J. Wild, *Nonlinear Regression*, Wiley, New York (1989).
Shao, J., and D. Tu, *The Jackknife and Bootstrap*, Springer-Verlag, New York (1995).
Shrager, R. I., "Chemical Transitions Measured by Spectra and Resolved Using Singular Value Decomposition," *Chemometrics Intelligent Lab. Syst.*, **1**, 59 (1986).
Shrager, R. I., and R. W. Hendler, "Titration of Individual Components in a Mixture with Resolution of Difference Spectra, pK's, and Redox Transitions," *Anal. Chem.*, **54**, 1147 (1982).
Smilde, A. K., R. Tauler, J. M. Henshaw, L. W. Burgess, and B. R. Kowalski, "Multicomponent Determination of Chlorinated Hydrocarbons Using a Reaction-Based Chemical Sensor. 3. Medium-Rank Second-Order Calibration with Restricted Tucker Models," *Anal. Chem.*, **66**, 3345 (1994).
Sylvestre, E. A., W. H. Lawton, and M. S. Maggio, "Curve Resolution Using a Postulated Chemical Reaction," *Technometrics*, **16**, 353 (1974).
Tauler, R., S. Fleming, and B. R. Kowalski, "Multivariate Curve Resolution Applied to Spectral Data from Multiple Runs of an Industrial Process," *Anal. Chem.*, **65**, 2040 (1993).
Tauler, R., A. Izquierdo-Ridorsa, R. Gargallo, and E. Casassas, "Application of a New Multivariate Curve Resolution Procedure to the Simultaneous Analysis of Several Spectroscopic Titrations of the Copper(II)-Polyinosinic Acid System," *Chemometrics Intelligent Lab. Syst.*, **27**, 163 (1995).
Tauler, R., A. K. Smilde, J. M. Henshaw, L. W. Burgess, and B. R. Kowalski, "Multicomponent Determination of Chlorinated Hydrocarbons Using a Reaction-Based Chemical Sensor. 2. Chemical Speciation Using Multivariate Curve Resolution," *Anal. Chem.*, **66**, 3337 (1994).
Weast, R. C., *Handbook of Chemistry and Physics*, 1st student ed., CRC Press, Boca Raton, FL (1988).
Workman, J. J. Jr., "Interpretive Spectroscopy of Near Infrared," *Appl. Spectrosc. Rev.*, **31**, 251 (1996).

Manuscript received Sept. 11, 1997, and revision received Aug. 17, 1998.